Metallurgical and Materials Engineering *Research paper*
Association of Metallurgical Engineers of Serbia AMES *https://doi.org/10.30544/841*

THERMAL TRANSPORT PROPERTIES AND MICROSTRUCTURE OF THE SOLID Bi-Cu ALLOYS

Dragan Manasijević[1], Ljubiša Balanović[1], Ivana Marković[1], Vladan Ćosović[2], Milan Gorgievski[1], Uroš Stamenković[1], Kristina Božinović[1]*

[1]University of Belgrade, Technical Faculty in Bor, Bor, Serbia
[2]University of Belgrade - Institute of Chemistry, Technology and Metallurgy, Njegoševa 12, 11001 Belgrade, Serbia

Received 12.05.2022
Accepted 23.09.2022

Abstract

Thermal transport properties of solid Bi-Cu alloys have been investigated over a wide composition range and temperature range ranging from 25 to 250 °C. The flash method was used to determine thermal diffusivity. Thermal diffusivity was discovered to decrease continuously with increasing temperature and bismuth content. The indirect Archimedean method was used to determine the density of the Bi-Cu alloys at 25 °C. The obtained results show that the density of the studied alloys decreases slightly as the copper content increases. Thermal conductivity of the alloys was calculated using measured diffusivity, density, and a calculated specific heat capacity. The thermal conductivity of the studied Bi-Cu alloys decreases with increasing temperature and bismuth content, similar to thermal diffusivity. SEM with energy dispersive X-ray spectrometry (EDS) and differential scanning calorimetry (DSC) were used to examine the microstructure and melting behavior of Bi-Cu alloys, respectively. The eutectic temperature was measured to be 269.9±0.1 °C, and the measured phase transition temperatures and heat effects were compared to thermodynamic calculations using the CALPHAD method.

Keywords: Bi–Cu system; microstructure; DSC; thermal conductivity.

*Corresponding author: Dragan Manasijević, *dmanasijevic@tfbor.bg.ac.rs*

Introduction

Bismuth alloys are being considered for use as Pb-free high-temperature [1] and low-temperature [2,3] solders due to their suitable melting interval. Bismuth is the least toxic heavy metal, but it has poor malleability, brittleness, and thermal conductivity [4,5]. It is rarely used as a structural material due to its poor mechanical and thermal properties. Copper and its alloys, on the other hand, have a wide range of applications due to their excellent electrical and thermal conductivities, outstanding corrosion resistance, ease of fabrication, and good strength and fatigue resistance [6]. Aside from soldering, bismuth and copper alloys are being investigated as potential materials for energy storage and surge protection [7] or as a catalyst for methane pyrolysis [8].

The Bi-Cu system is a simple eutectic system with a eutectic point of 270.5 ° C. [9], which is very close to the melting point of pure bismuth (degenerated phase equilibrium). In the solid state, the mutual solubility of bismuth and copper is negligible [10]. Thermodynamic properties and phase relationships in the Bi-Cu system have been extensively studied [9,10], but data on the thermophysical properties of these alloys are still sporadic in the literature. *Gomez et al.* [11], *Oleksiak et al.* [12], and *Pstrus and Fima* [8] measured the densities and surface tensions of liquid Bi-Cu alloys. There appears to be no data available on the thermal transport properties of Bi-Cu alloys.

As a contribution toward a more complete understanding of thermal transport properties of the Bi-Cu alloys, in the present paper four Bi-Cu alloys with experimentally obtained compositions $Bi_{85.9}Cu_{14.1}$, $Bi_{72.5}Cu_{27.5}$, $Bi_{54.6}Cu_{45.4}$, $Bi_{30.7}Cu_{69.3}$ (in at.%) were studied using several experimental techniques. Thermal diffusivity and thermal conductivity were obtained in wide composition and temperature ranges. In addition, microstructure analysis using SEM and determination of phase transition temperatures using the DSC method were conducted.

Materials and methods

Induction melting of pure Bi (99.995%, Alfa Aesar) and Cu (99.999%, Alfa Aesar) in graphite crucibles in a high-purity Ar atmosphere produced the studied alloys. To ensure microstructure homogeneity, the samples were re-melted several times.

The SEM (Tescan VEGA 3LMU) with the EDS was used to analyze the microstructures and chemical compositions of the samples (Oxford Instruments X-act). SEM-EDS analysis was performed with an accelerating voltage of 20 kV. An EDS area and point analysis was used to determine the overall compositions of the alloys as well as the compositions of coexisting phases within each alloy. The samples were prepared using a traditional metallographic procedure that included grinding, polishing, and cleaning in an ultrasonic bath, but no surface etching. Backscattered electron mode (BSE) SEM microstructure images were captured on the surfaces of the prepared samples.

The xenon-flash method was used with the TA Instruments compact benchtop apparatus to measure thermal diffusivity from 25 to 250 °C (Discovery Xenon Flash DXF-500). More information on the fundamental theoretical concepts and practical procedures underlying the used xenon-flash method can be found in [13-17]. The cast Cu-Bi alloy samples were machined into round disks (12.6 mm in diameter and 2 mm thick, with two ground plane parallel end-faces) before being annealed at 200 °C for 48 hours. The prepared disc-shaped samples were then placed in the DXF-500 instrument's vacuum

furnace and heated to measurement temperatures (25°C, 50°C, 100°C, 150°C, 200°C, and 250°C) at a constant heating rate (10 °Cmin^{-1}).

Specific heat capacity values were calculated using the CALPHAD method, and densities of the investigated alloys at room temperature were determined using the indirect Archimedean method [14,16] with distilled water (0= 0.99679 kgm^{-3}) and a Mettler Toledo electronic instrument.

Thermal conductivity of the alloys was subsequently calculated using the experimentally determined and calculated values of thermal diffusivity, density and specific heat capacity, following the equation [13]:

$$\lambda = \alpha \cdot \rho \cdot Cp \qquad 1$$

where λ represents thermal conductivity (Wm^{-1}K^{-1}), α is the measured thermal diffusivity (m^{2}s^{-1}), ρ is the value of density (kgm^{-3}), and *C*p is the calculated specific heat capacity (Jg^{-1}K^{-1}) of the studied alloys.

TA Instruments simultaneous thermal analyzer (SDT Q600) was employed to record DSC data and to provide information on phase transformations and correlated heat effects. The DSC device was firstly calibrated before measuring. As reference material, an alumina plate was used. The mass of the each investigated alloy sample was about 30 mg, while the heating rate was 5 °Cmin^{-1}.

For an easier review of the experimental procedure, a flow diagram of the experimental procedure is given in Fig. 1.

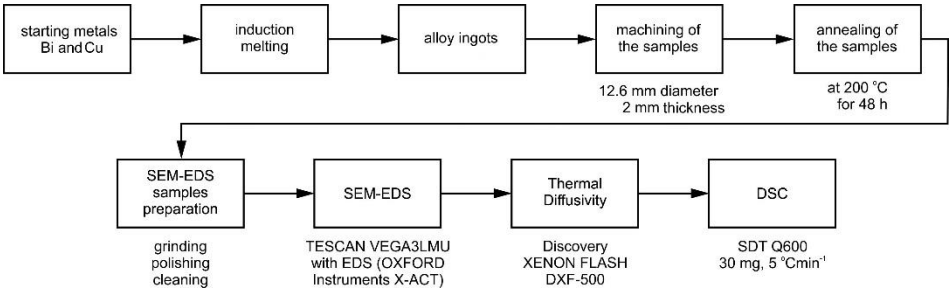

Fig. 1. Flow chart of the experimental procedure.

Results and discussion

Microstructure observation

SEM micrographs, illustrating microstructures of the investigated $Bi_{85.9}Cu_{14.1}$, $Bi_{72.5}Cu_{27.5}$, $Bi_{54.6}Cu_{45.4}$, and $Bi_{30.7}Cu_{69.3}$ alloys under different magnifications, are given in Figs. 2-5.

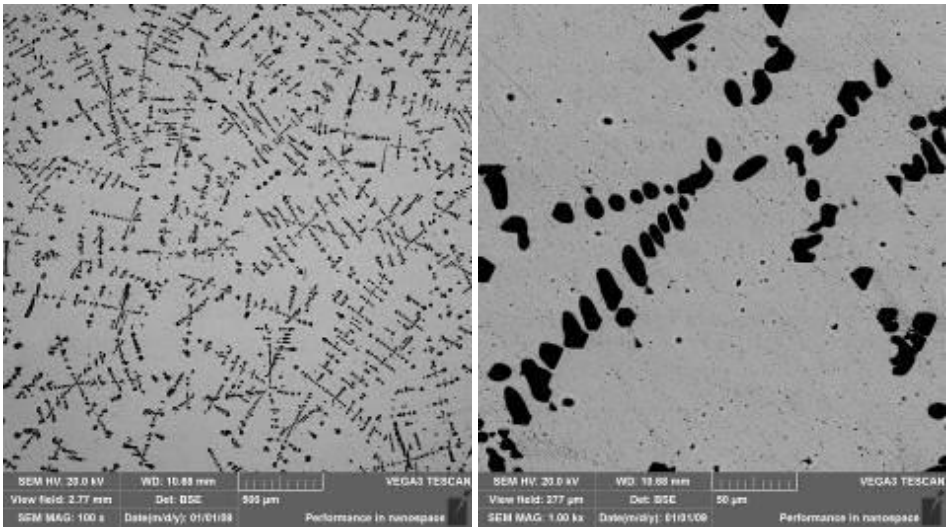

(a) *(b)*

Fig. 2. SEM image of the $Bi_{85.9}Cu_{14.1}$ alloy: (a) magnification 100X; (b) magnification 1000X.

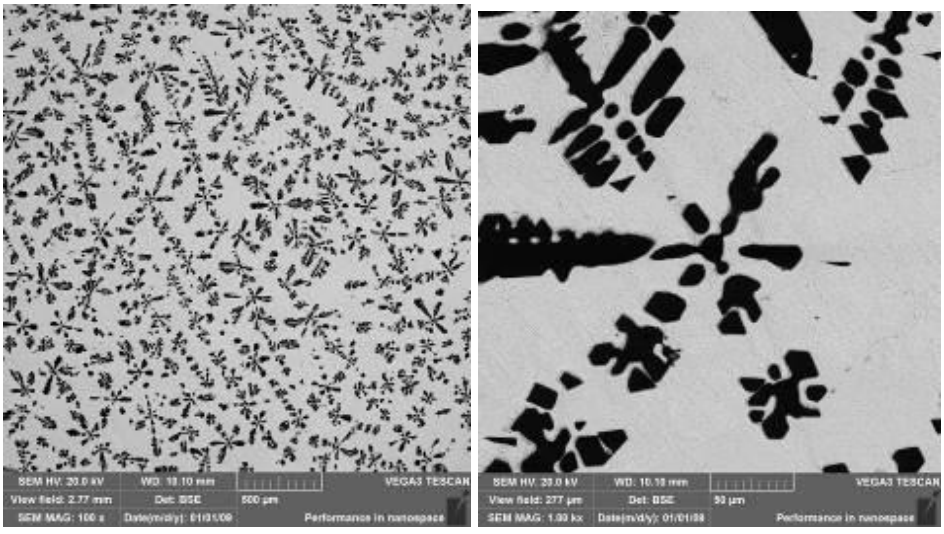

(a) *(b)*

Fig. 3. SEM image of the $Bi_{72.5}Cu_{27.5}$ alloy: (a) magnification 100X; (b) magnification 1000X.

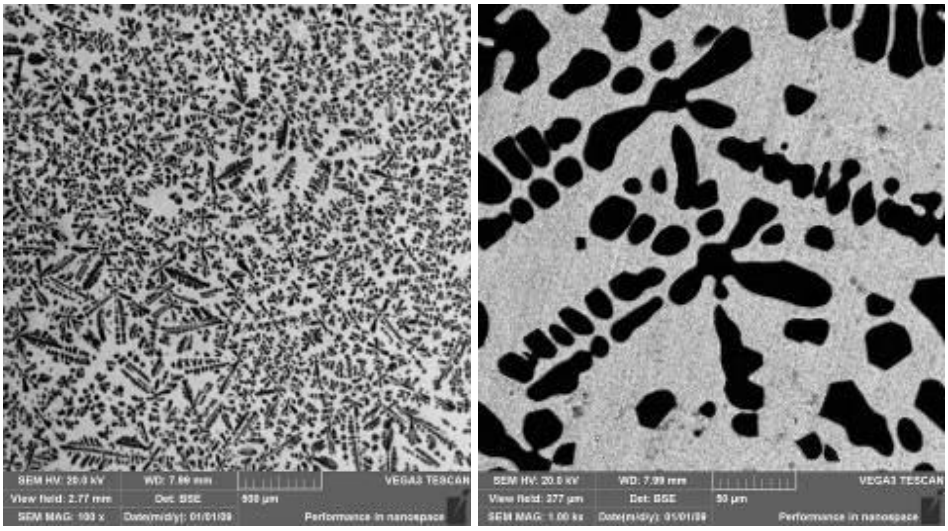

(a) *(b)*

Fig. 4. SEM image of the $Bi_{54.6}Cu_{45.4}$ alloy: (a) magnification 100X; (b) magnification 1000X.

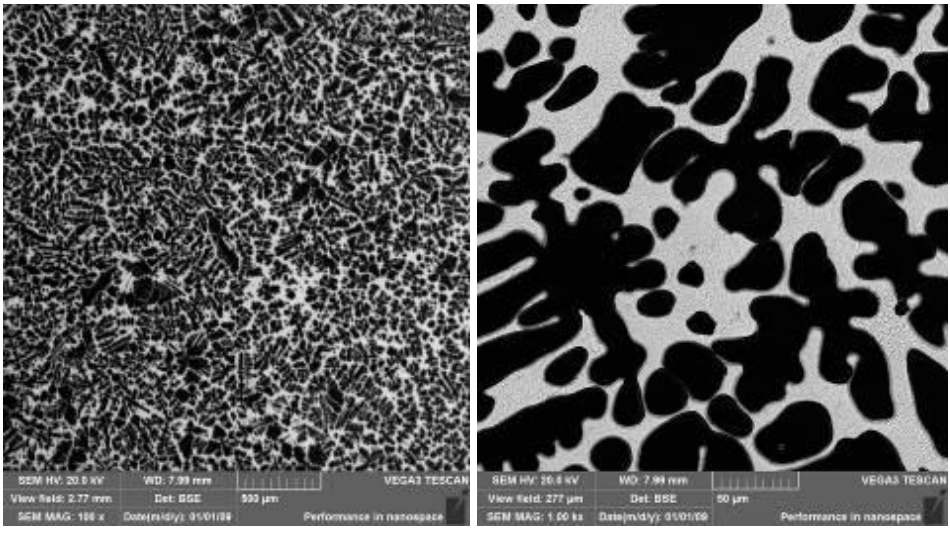

(a) *(b)*

Fig. 5. SEM image of the $Bi_{30.7}Cu_{69.3}$ alloy: (a) magnification 100X; (b) magnification 1000X.

Alloys have a highly homogeneous microstructure that can be seen throughout the samples (Figs. 2-5). The microstructure of all investigated alloys shows primary dark dendrites bounded by the bright phase. The EDS analysis results show that the dark dendrites are almost pure Cu, i.e. (Cu) phase, whereas the bright phase is the Bi-based (Bi)+(Cu) eutectic. Table 1 shows the observed microstructure, identified phases, and microconstituents, as well as their compositions.

The eutectic is composed of a Cu-rich phase dispersed in a Bi-rich phase, as revealed by higher magnification SEM images (Figs. 1b-4b). With increasing bismuth content in the alloys, the primary Cu-rich dendrites become oblong and non-ramified. The rounded shape of the primary (Cu) phase is thought to be the result of dendritic growing crystal degeneration (Fig. 2). With decreasing bismuth content, the oblong Cu dendrites shorten and exhibit clear primary and secondary arms (Figs. 3-5); additionally, the number of primary Cu-rich dendrites increases.

Table 1. The results of SEM-EDS analysis.

Sample/at.%	Microstructure	Identified phases and microconstituents	Composition/at.%	
			Bi	Cu
$Bi_{85.9}Cu_{14.1}$	Primary dendrites of (Cu) in the Bi-rich (Bi)+(Cu) eutectic base	(Cu)	-	100.0
		(Bi)+(Cu) eutectic	98.2±0.5	1.8±0.2
$Bi_{72.5}Cu_{27.5}$	Primary dendrites of (Cu) in the Bi-rich (Bi)+(Cu) eutectic base	(Cu)	-	100.0
		(Bi)+(Cu) eutectic	98.1±0.6	1.9±0.2
$Bi_{54.6}Cu_{45.4}$	Primary dendrites of (Cu) in the Bi-rich (Bi)+(Cu) eutectic base	(Cu)	-	100.0
		(Bi)+(Cu) eutectic	98.4±0.5	1.6±0.3
$Bi_{30.7}Cu_{69.3}$	Primary dendrites of (Cu) in the Bi-rich (Bi)+(Cu) eutectic base	(Cu)	-	100.0
		(Bi)+(Cu) eutectic	98.4±0.7	1.6±0.2

Differential scanning calorimetry measurements

Differential scanning calorimetry was used to identify phase transition temperatures and measure heat effects. The DSC results were analyzed in accordance with the literature recommendations for interpreting heat flux DSC curves of binary metallic systems [18]. The temperature of the eutectic reaction was designated as the onset temperature of the first DSC peak on the heating curve, and the temperature of the liquidus was designated as the peak temperature of the second thermal event during heating. DSC heating runs were repeated five times for each of the tested samples, and average values were calculated using the results of the repeated tests. Figure 6 shows examples of DSC heating curves for all Bi-Cu samples studied.

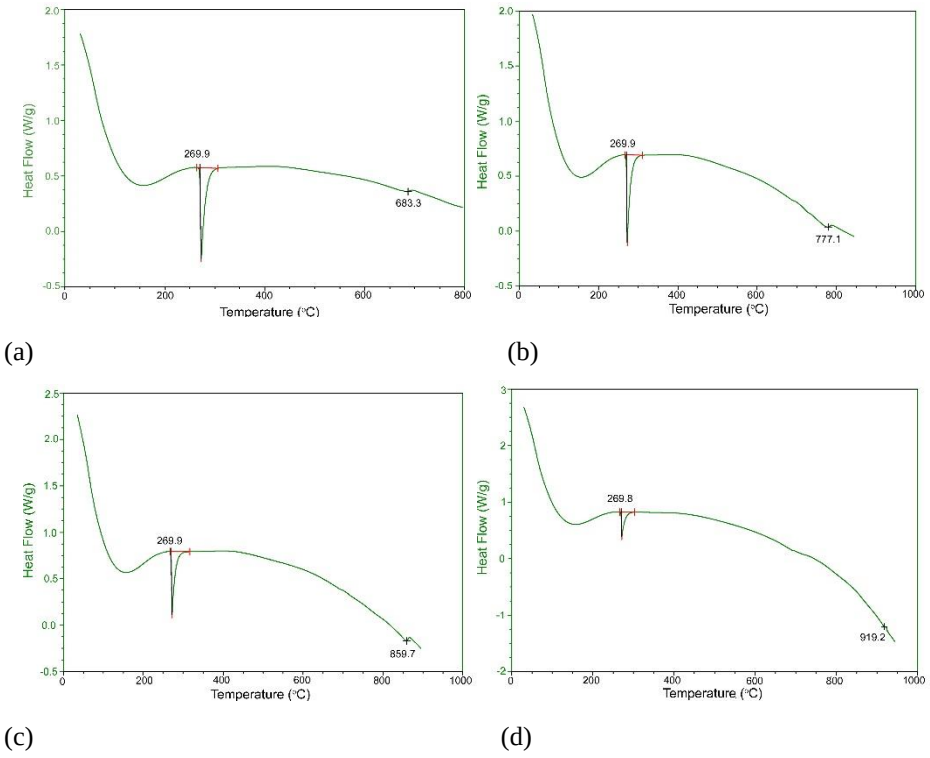

Fig. 6. DSC heating curve: (a) $Bi_{85.9}Cu_{14.1}$ alloy; (b) $Bi_{72.5}Cu_{27.5}$ alloy; (c) $Bi_{54.6}Cu_{45.4}$ alloy; (d) $Bi_{30.7}Cu_{69.3}$ alloy.

Table 2 presents a comparison between the experimental results of DSC measurements and results of thermodynamic calculations. Average values of phase transition temperatures and values of heat of eutectic reaction, together with standard uncertainties were evaluated from the repeated measurements.

Table 2. Comparison between the results of DSC measurements and thermodynamic calculations for the Bi–Cu eutectic alloys

Alloy composition / at.%	Experimentally determined temperature of eutectic reaction / °C	Calculated temperature of eutectic reaction / °C	Measured heat of eutectic transition / Jg^{-1}	Calculated enthalpy of eutectic transition / Jg^{-1}	Experimentally determined liquidus temperature / °C	Calculated liquidus temperature / °C
$Bi_{85.9}Cu_{14.1}$	269.9±0.1	270.5	46.6±0.2	52.2	683.3±1.1	644.4
$Bi_{72.5}Cu_{27.5}$	269.9±0.1	270.5	42.6±0.2	50.0	777.1±1.5	742.2
$Bi_{54.6}Cu_{45.4}$	269.9±0.1	270.5	34.7±0.1	43.6	859.7±1.6	825.2
$Bi_{30.7}Cu_{69.3}$	269.8±0.1	270.5	20.4±0.1	32.4	919.2±2.0	903.1

The presented results (Table 2) show that the value of heat of the eutectic reaction gradually decreases with increasing copper content within the alloys, and that it is highest for $Bi_{85.9}Cu_{14.1}$ alloy (46.6 Jg^{-1}). The measured values are to some extent lower than the theoretical values of latent heat of melting (enthalpy of melting) calculated by using a thermodynamic database [9,19].

The optimized phase diagram of Bi-Cu system, calculated by using thermodynamic parameters from Teppo et al. [9], included in the COST 531 lead-free solder database [19], is presented in Fig. 7 together with the obtained DSC results for comparison.

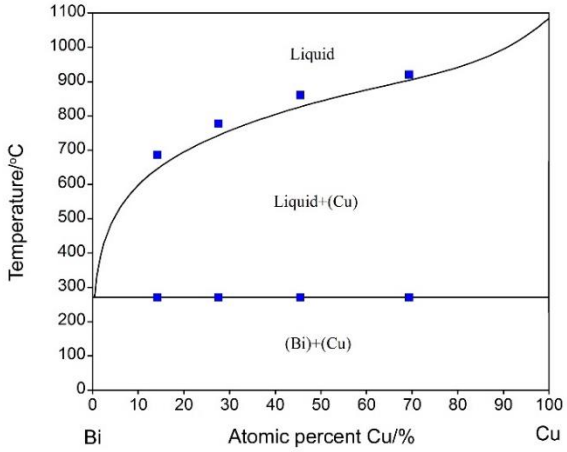

Fig. 7. The optimized phase diagram of the Bi-Cu system [9,19] with the DSC results from the present work.

There is a close agreement between the measured temperatures of the eutectic reaction (average measured temperature 269.9 °C) (Table 2) and the calculated Bi-Cu phase diagram temperature of the eutectic reaction (270.5 °C) (Fig 7). However, the liquidus temperatures obtained experimentally are significantly higher than the related temperatures determined by the phase diagram.

Thermal conductivity measurements

Thermophysical properties of pure Bi and Cu are presented in Table 3.

Table 3. Thermophysical properties of pure Bi and Cu [6].

Metal	Melting point /°C	Latent heat of fusion/ Jg^{-1}	Density/gcm^{-3}	Specific heat capacity/$Jg^{-1}K^{-1}$	Thermal conductivity /$Wm^{-1}K^{-1}$
Bi	271.4	53.976	9.808 at 25 °C	0.122 at 25 °C	8.2 at 25 °C
Cu	1084.88	205.0	8.93 at 20 °C	0.384 at 25 °C	398.0 at 27 °C

As can be seen, bismuth has very low thermal conductivity (8.2 $Wm^{-1}K^{-1}$ at 20 °C). In contrast to bismuth, after silver, copper has the highest thermal conductivity among all metals (398.0 $Wm^{-1}K^{-1}$ at 27 °C). Furthermore, copper has much higher melting point, latent heat of fusion, specific heat capacity, and thermal conductivity than bismuth.

Thermal conductivity of solid Bi-Cu alloys was determined in this study over a wide composition range and at temperatures ranging from 25 to 250 °C. The flash method, which directly measures thermal diffusivity, was used. Following the thermal diffusivity measurements, thermal conductivity was calculated using the density and specific heat capacity data of the investigated materials (Eq. 1).

Table 4. Specific heat capacity, thermal diffusivity, and thermal conductivity of the investigated Bi–Cu alloys in the temperature range 25-250 °C.

Alloy composition /at.%	Temperature, T/°C	Calculated specific heat capacity, $Cp/Jg^{-1}K^{-1}$	Measured thermal diffusivity, α/mm^2s^{-1}	Thermal conductivity, $\lambda/Wm^{-1}K^{-1}$
$Bi_{85.9}Cu_{14.1}$	25	0.13	7.84	9.99
	50	0.14	7.22	9.91
	100	0.14	6.60	9.06
	150	0.14	6.03	8.27
	200	0.15	5.54	8.14
	250	0.15	4.52	6.64
$Bi_{72.5}Cu_{27.5}$	25	0.15	12.23	17.81
	50	0.15	11.57	16.85
	100	0.15	10.48	15.26
	150	0.16	9.63	14.96
	200	0.16	8.94	13.89
	250	0.17	7.97	13.16
$Bi_{54.6}Cu_{45.4}$	25	0.18	14.73	25.43
	50	0.18	13.82	23.86
	100	0.18	12.55	21.66
	150	0.18	11.55	19.94
	200	0.19	10.8	19.68
	250	0.2	10.11	19.39
$Bi_{30.7}Cu_{69.3}$	25	0.23	25.27	54.23
	50	0.23	24.33	52.21
	100	0.24	22.47	50.31
	150	0.24	21.04	47.11
	200	0.25	19.91	46.44
	250	0.25	19.04	44.41

Firstly, alloys' densities at room temperature were measured using the buoyancy method based on Archimedes' principle with an estimated uncertainty of ± 1%. The obtained density values for the $Bi_{85.9}Cu_{14.1}$ alloy, $Bi_{72.5}Cu_{27.5}$ alloy, $Bi_{54.6}Cu_{45.4}$ alloy, and $Bi_{30.7}Cu_{69.3}$ alloy are 9.80, 9.71, 9.59, and 9.33 gcm^{-3}, respectively. It was assumed that the densities of the alloys are approximately constant in the temperature range studied.

The CALPHAD method [20] and the thermodynamic COST 531 lead-free solder database [19] were used to calculate the specific heat capacities of the alloys under

consideration. The calculated specific heat capacity values were checked for accuracy (± 5%) by comparing them to the related measured values obtained at room temperature using the xenon-flash technique (pure bismuth was used as a reference material).

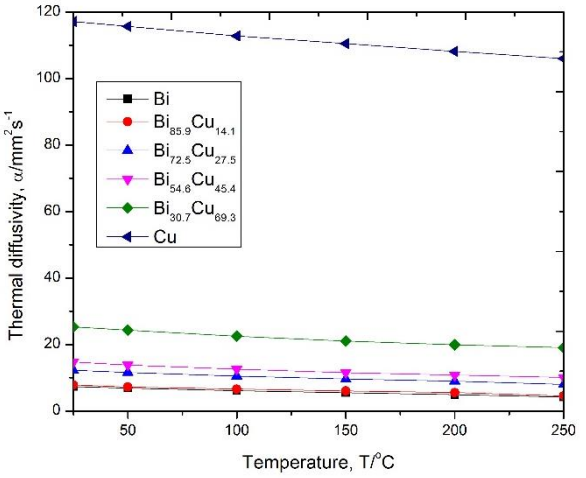

(a)

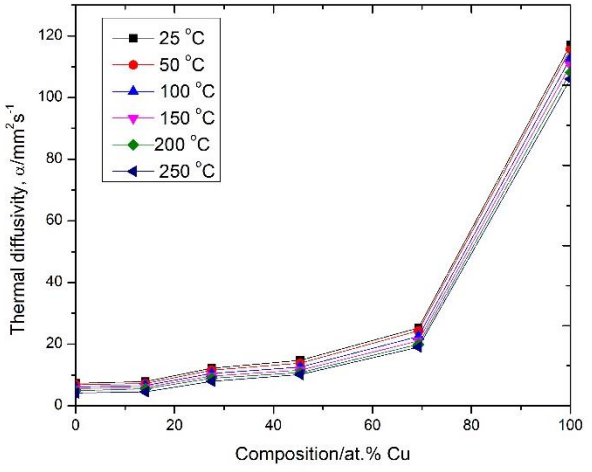

(b)

Fig. 8. Thermal diffusivity variations for the studied Bi-Cu alloys and the pure constitutive metals Bi and Cu: (a) with temperature; (b) with composition.

The obtained values of thermal diffusivity, specific heat capacity, and thermal conductivity for the Bi-Cu alloys investigated in the temperature range from 25 to 250 °C are given in Table 4. The standard uncertainty (0.68 level of confidence) for the thermal diffusivity measurements is ± 3% [21]. The total standard uncertainty for the thermal conductivity is estimated to be ± 6% [14].

The obtained results (Table 4) show that the value of specific heat capacity gradually increases as copper content increases. The variations in thermal diffusivity with temperature and composition are depicted in Figs. 8a and 8b, respectively. It can be seen that the thermal diffusivity of all alloys studied decreases slightly with increasing temperature. Thermal diffusivity increases with increasing copper content, as expected, and the observed increase is more pronounced at higher copper contents. At 25 °C, thermal diffusivity increases from 7.84 mm^2s^{-1} for the $Bi_{85.9}Cu_{14.1}$ alloy up to 25.27 mm^2s^{-1} for the $Bi_{30.7}Cu_{69.3}$ alloy.

Thermal conductivity dependence on temperature is given in Fig. 9.

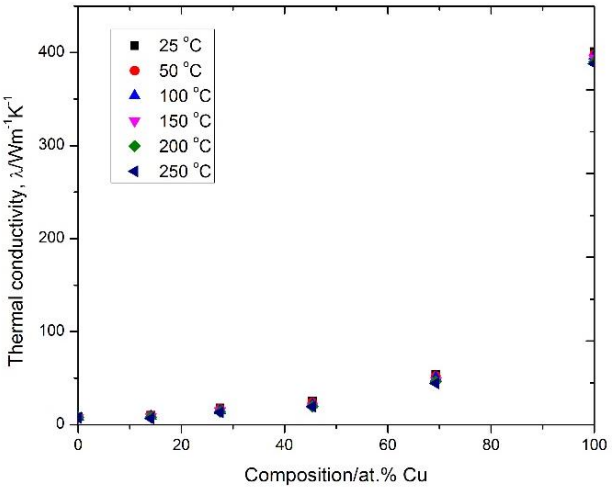

Fig. 9. Thermal conductivity dependence on composition for the investigated Bi-Cu alloys and the pure constitutive metals Bi and Cu at the studied temperatures.

According to Fig. 9, the thermal conductivity of the studied solid Bi-Cu alloys deviates significantly from a linear mixing rule. Furthermore, similar to thermal diffusivity, the thermal conductivity of solid Bi-Cu alloys decreases slightly with increasing temperature.

Conclusion

The effects of temperature and composition on the thermal transport properties of the solid Bi-Cu alloys were systematically investigated. It was noticed that specific heat capacity of the alloys gradually increases with increasing copper content and temperature. Expectedly, density of the alloys increases with increasing bismuth content. The obtained results also show that both thermal diffusivity and thermal conductivity decrease with increasing temperature and bismuth content. Metallographic observations have revealed that microstructure of the each investigated Bi-Cu alloy includes primary dendrites of nearly pure Cu in the Bi-rich eutectic base. The experimentally obtained eutectic temperature of 269.9 °C was found to be in very close agreement with the literature and the calculated thermodynamic data.

Acknowledgment

The research presented in this paper was done with the financial support of the Ministry of Education, Science and Technological Development of the Republic of Serbia, within the funding of the scientific research work at the University of Belgrade, Technical Faculty in Bor, and at University of Belgrade - Institute of Chemistry, Technology and Metallurgy according to the contracts with registration numbers 451-03-68/2022-14/200131 and 451-03-68/2022-14/200026, respectively.

References

[1] M. Yu, K. Matsugi, Z. Xu, Y. Choi, J. Yu, S. Motozuka, Y. Nishimura, K. I. Suetsugu: Mater Trans, 59 (2018) 303-310.
[2] H. Lee, K.-S. Choi, Y.-S. Eom, H.-C. Bae, J. H. Lee: ETRI J, 38 (2016) 1163–1171.
[3] Y. Goh, A.S.M.A. Haseeb, M.F.M. Sabri: Electrochim Acta, 90 (2013) 265–273.
[4] J. E. Spinelli, B. L. Silva, A. Garcia: Mater Des, 58 (2014) 482-490.
[5] J. M. Song, H. Y. Chuang, T.X. Wen: Metall Mater Trans A, 38 (2007) 1371-1375.
[6] ASM International Handbook Committee: Properties and selection: nonferrous alloys and special-purpose materials, 2, ASM international, Materials Park, OH, 1990.
[7] S. P. Singh, B. K. D. Barman, P. Kumar: Mater Sci Eng A, 677 (2016) 140-152.
[8] J. Pstruś, P. Fima: Metall Mater Trans A, 53 (2022) 1-15.
[9] O. Teppo, J. Niemela, P. Taskinen: Report TKK-V-B50, Helsinki University of Technology, Finland, 1989.
[10] L. S. Chang, B. B. Straumal, E. Rabkin, W. Gust, F. Sommer: J Phase Equilib, 18 (1997) 128-135.
[11] M. Gomez, L. M. Garin, H. Ebert, P. Bedon, P. Desre: Z Met kd, 67 (1976) 131-134.
[12] R. Burdzik, B. Oleksiak, J. Wieczorek, J. Łabaj, A. Blacha-Grzechnik: Arch Metall Mater, 59 (2014) 281-285.
[13] W. J. Parker, R. J. Jenkins, C. P. Butler, G. L. Abbott: J Appl Phys, 32 (1961) 1679-1684.
[14] D. Manasijević, L. Balanović, I. Marković, M. Gorgievski, U. Stamenković, K. Božinović: Thermochim Acta, 702 (2021) 178978. 2021.
[15] D. Manasijević, L. Balanović, I. Marković, M. Gorgievski, U. Stamenković, A. Đorđević, D. Minić, V. Ćosović: Solid State Sci, 119 (2021) 106685.
[16] D. Manasijević, L. Balanović, I. Marković, D. Minić, M. Premović, A. Đorđević, M. Gorgievski, U. Stamenković: J Therm Anal Calorim, 147 (2022) 1965-1972.
[17] D. Manasijević, L. Balanović, V. Ćosović, D. Minić, M. Premović, M. Gorgievski, U. Stamenković, N. Talijan: Metall Mater Eng, 25(4) (2019) 325-334.
[18] W. J. Boettinger, U. R. Kattner, K. W. Moon, J. H. Perepezko: Methods for Phase Diagram Determination, First edition, Elsevier, Kindlington, Oxford, 151-221.
[19] A. Kroupa, A. T. Dinsdale, A. Watson, J. Vrestal, J. Vízdal, A. Zemanová: JOM, 59 (2007) 20-25.
[20] H. L. Lukas, S. G. Fries, B. Sundman: Computational Thermodynamics: the Calphad Method, First edition, Cambridge University Press, Cambridge, 2007.
[21] L. Huang, S. Liu, Y. Du, C. Zhang: Calphad, 62 (2018) 99-108.